Composites Part B 177 (2019) 107385

Contents lists available at ScienceDirect

Composites Part B

journal homepage: www.elsevier.com/locate/compositesb

Predicting the stacking sequence of E-glass fiber reinforced polymer (GFRP) epoxy composite using terahertz time-domain spectroscopy (THz-TDS) system

Dong-Woon Park [a], Gyung-Hwan Oh [a], Hak-Sung Kim [a,b,*]

[a] Department of Mechanical Convergence Engineering, Hanyang University, 222 Wangsimni-ro, Seongdong-gu, Seoul, Republic of Korea
[b] Institute of Nano Science and Technology, Hanyang University, 222 Wangsimni-ro, Seongdong-gu, Seoul, Republic of Korea

ARTICLE INFO

Keywords:
Terahertz wave
Non-destructive testing
Laminated composites
Electrical properties
Stacking sequence
Fiber direction

ABSTRACT

A terahertz time-domain spectroscopy (THz-TDS) system was used for measuring and predicting stacking sequence of laminated composites. The THz wave's penetration behavior in emissivity (E)-glass fiber reinforced polymer epoxy composites was analyzed. The relationship between polarization angle of THz radiation to fiber direction of the composites and dielectric constant in THz frequency range was formulated using a two-dimensional transformation matrix. Then, the dielectric constants of arbitrarily laminated composite plates were calculated by combining the transformation matrix via laminating rule. The dielectric constants of the arbitrarily laminated composites were measured and compared with those of the developed theoretical models. It was found that the THz waves could be successfully used to predict the stacking sequence of the laminated composites with 0.25% error.

1. Introduction

Continuous fiber-reinforced polymers (FRPs) composites are emerging as alternatives to metal materials in many industry fields including aerospace, automobiles, and sports goods [1–3]. The use of composites provides definite advantages such as lower weight of the structure, lower production cost, and superior mechanical properties compared to the metal materials [4–6]. Since the mechanical properties of the FRPs composites vary depending on stacking angle of laminated composites, the stacking angle is designed with consideration for their application and purpose [7–9].

Among the various the FRPs composites, emissivity (E)-glass/epoxy (GFRP) composite laminates have attracted attention due to their superior mechanical properties [10]. The GFRP composites have been widely employed in a variety of automotive composite components, including bumper beams, hoods, and leaf springs [11–13]. In all these applications, fiber orientation of the GFRP composite laminates are important factors for determining the mechanical performance of the automobile components.

Resin transfer molding (RTM), vacuum-assisted resin transfer molding (VARTM), and compression molding process have been widely used for fabrication of the FRPs composites [14–16]. During forming complex shaped product with the FRPs composites, the fiber orientation of the composites can be unexpectedly distorted. Depending on the fiber orientation, the mechanical properties of the FRPs composites can be changed more than two times [17]. Therefore, the complex shaped product with the FRPs composites could have different mechanical properties from initial design. Therefore, the fiber orientation in the FRP composites needs to be checked and monitored to guarantee the initial design using appropriate method [18,19].

Consequently, the need for non-destructive testing (NDT) and evaluation (NDE) methods is recently increasing for the FRPs composites [20–22]. To investigate the fiber orientation, many inspection methods using ultrasonic wave and electromagnetic wave such as microwave, an active infrared thermography technique, and X-ray have been studied [23–29]. Since the ultrasonic inspection methods require a liquid medium, e.g., water, moisture absorption in the composites might cause their mechanical properties to deteriorate [23]. Using the active infrared thermography technique, the study for investigating fiber orientation on the surface of the FRPs composites was conducted by an analysis of the thermal propagation pattern [24]. However, the active infrared thermography technique can induce a local-heat-defect and extract the fiber orientation information only from the surface of the composite laminates. Using microwave, the orientation of various type of the fibers has

* Corresponding author. Department of Mechanical Convergence Engineering, Hanyang University, 222 Wangsimni-ro, Seongdong-gu, Seoul, Republic of Korea.
E-mail address: kima@hanyang.ac.kr (H.-S. Kim).

https://doi.org/10.1016/j.compositesb.2019.107385
Received 8 June 2019; Received in revised form 12 August 2019; Accepted 26 August 2019
Available online 28 August 2019
1359-8368/

been inspected [25–27]. However, it was found that the sensitivity for detecting glass-fiber orientation is too low because the difference of electro-magnetic properties between glass fiber and epoxy resin is small in microwave frequency band [30]. The reflection or transmission of two orthogonal polarized microwave were measured, and their ratio was calculated to improve the sensitivity for inspecting fiber orientation. This may cause inconvenience in arraying and installing the optical system. Also, the leakage of the microwaves should be restricted below a certain level as it is dangerous to human health. In addition, micro X-ray CT inspection methods can scan the fiber and analysis its orientation with high resolution, because X-ray has the relatively short wavelength compared to ultrasonic and microwave [28,29]. However, due to its ionizing characteristic, the X-ray have a high energy and therefore, are harmful to the human body; hence, additional safety equipment is needed to protect the human body from X-ray exposure.

On the other hand, inspection methods using terahertz (THz) wave can easily inspect samples at relatively low energy levels without a medium, e.g., water [31,32]. Additionally, THz radiation has non-contact, non-invasive, and non-ionizing modalities to characterize various non-metallic materials [33,34]. The terahertz radiation's frequency spectrum extends from 0.1 to 10 THz, which lies between the microwave and infrared frequencies; the wavelength range is from 3 mm to 30 μm in free space [35]. The inspection methods using the THz wave are emerging as a promising technique in the industrial, medical, and security [36–38]. The THz inspection methods in the industrial field have been actively studied for materials such as composites, cement, semiconductors, and wooden objects [39–42].

In this work, a terahertz time-domain spectroscopy (THz-TDS) system was used to inspect stacking sequence and fiber direction of GFRP composite laminates. The THz wave's penetration behavior with the GFRP composites were investigated using experimental and theoretical analyses, as shown in Fig. 1. In the THz frequency range, the electromagnetic properties of unidirectional GFRP composite were measured by changing the polarization angle of THz radiation to the fiber direction of composites. The dielectric constants from the experimental results were correlated with the theoretical analysis. Theoretical models for predicting the dielectric constants were suggested to demonstrate the dielectric constant behavior of laminated composites with an arbitrary stacking angle. To non-destructively inspect the stacking sequence of GFRP composite, an algorithm for predicting the dielectric constants was suggested and verified based on the measured dielectric constant.

2. Experiment

2.1. THz-TDS system

A terahertz time-domain spectroscopy (THz-TDS) system was used to measure the electro-magnetic property of the GFRP composite laminates as shown in Fig. 2. The THz-TDS system consists of an emitter module, a detector module, a femto-second laser-generation module, and optical device, e.g., reflectors, beam splitters, and lenses. A commercial THz-TDS system (FiCO™, Zomega Terahertz Corp.) is shown in Fig. 2. The THz radiation of THz measurement system have a frequency in the electro-magnetic spectrum region from 0.1 to 3.0 THz. The maximum value of signal-to-noise ratio (SNR) is 60 dB, which is appropriate for measuring the material parameter data. The value of SNR is kept over 50 dB from 0.2 THz to 0.8 THz. The relative humidity in the THz-TDS system installation was maintained under 5% to eliminate any possible the effect of water-vapor absorption [43]. The temperature in the THz-TDS system was maintained at 25 °C to obtain stable laser oscillations.

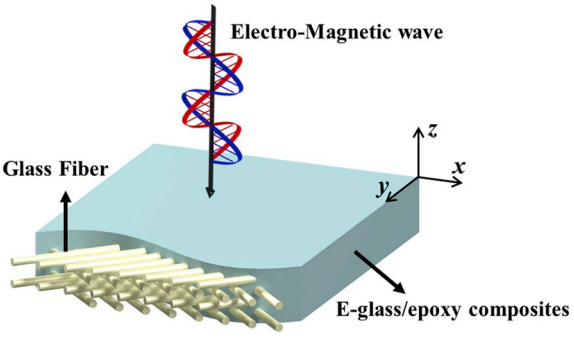

Fig. 1. The schematic of inspecting for laminate sequence of composite using THz inspection system.

Due to diffraction effects caused by the incidence angle of THz wave and multiple reflections via the sample, inaccuracies can occur when measuring the terahertz signals [44]. To minimize these drawbacks, the THz-TDS system's transmission-mode setup was used to collect the materials' property data as shown in Fig. 3. To measure the terahertz characteristics of the sample, the THz radiation from an emitter was propagated in a unidirectionally polarized state. A set of mirrors was used to focus the THz radiation on the sample. Then, it was gathered by another set of mirrors and collected in the detector. The measurements were repeatable because a system was installed that averaged 500 scans for each data set and normalized their frequency spectra in less than 1 s.

2.2. Sample preparation

The GFRP epoxy composite laminates were manufactured using a vacuum bagging. Unidirectional E-glass/epoxy pre-impregnated material (UGN160B, SK Chemical) was used to make the specimens; the properties of the prepreg are listed in Table 1. A unidirectionally laminated composite specimen and three different composite specimens with $[\pm 30^\circ]_{3s}$, $[+45^\circ/0^\circ/-45^\circ]_{2s}$, and $[+60^\circ/0^\circ/-60^\circ]_{2s}$ stacking sequences were prepared by laminating 12 plies of the prepregs. As shown in Fig. 4, the stacked prepregs were cured under the curing cycle and air pressure of 0.6 MPa. The planar composite specimens had a thickness of 1.63 ± 0.01 mm.

2.3. Measurement properties

In the THz-TDS system transmission mode, the prepared specimens were placed in the focus of the emitter and detector so that THz pulses could be irradiated vertically onto the specimen. As shown in Fig. 5, while the polarization angle (θ) of the THz radiation to the fiber direction of composite was changed from 0° to 90° in 10° increments, the electro-magnetic (EM) properties of the composite were measured. The electric-field vector shows the polarized direction of the THz radiation. To minimize the error, the EM properties in the 0.2–0.8 THz frequency range were used where value of SNR is over 50 dB [45].

3. Theory

3.1. Calculation of the complex permittivity

The electric field of the THz wave emitted by the THz-TDS system is dependent on the time. The complex relative permittivity can be calculated using the THz signal difference between the reference and the sample. For a transmission measurement of the THz-TDS system, the reference data of the THz signal is typically measured without sample. By Fourier transformation, time-dependent data of the electric field $E(t)$ is transformed to the circular frequency-dependent data ($E(\omega)$) below as,

$$E(\omega) = \int_{-\infty}^{\infty} E(t) e^{-i\omega t} dt \tag{1}$$

The calculation result from Eq (1) is complex number composed of real and imaginary parts. From Euler's formula, it can be transformed to express the magnitude (A) and the phase (ϕ) of the electric field as a function of the frequency ($E(\omega)$). The complex transmission coefficient

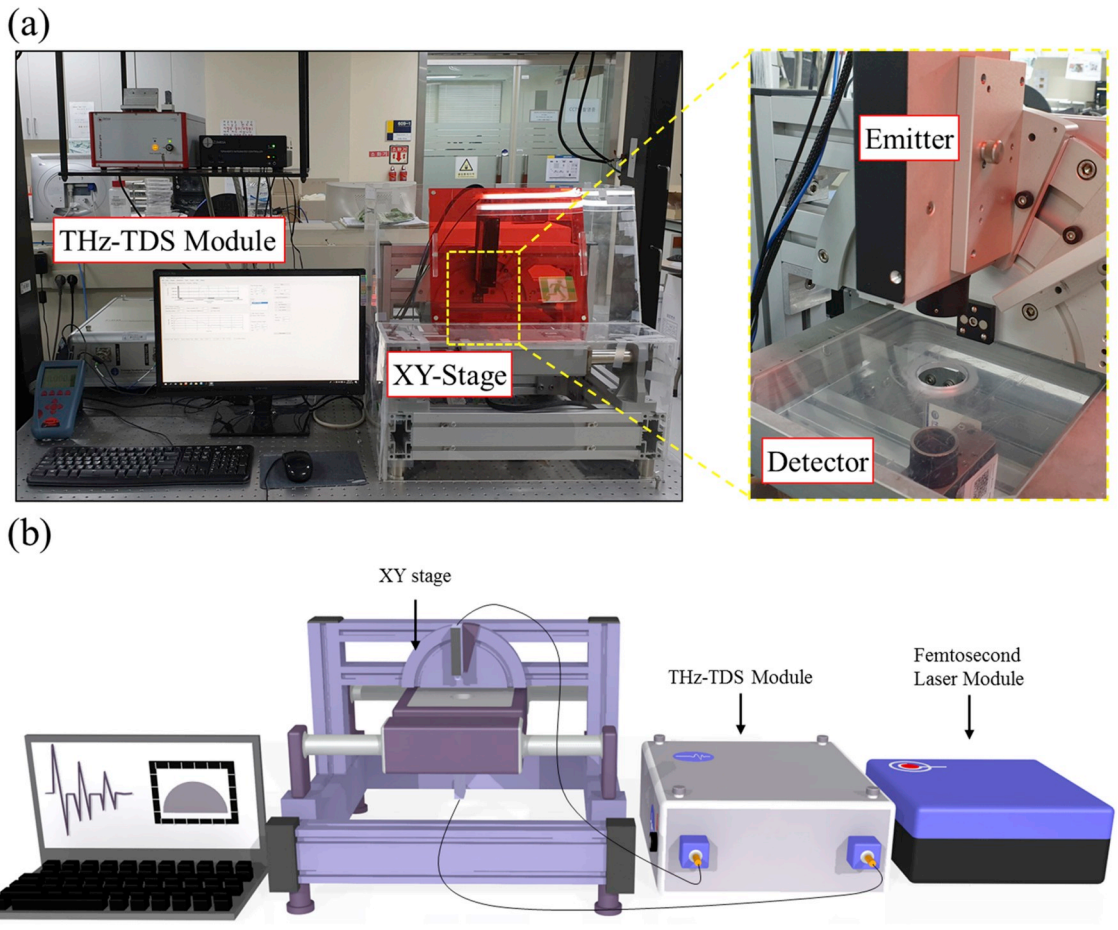

Fig. 2. (a) The photo of experimental set up for measurement, and (b) the schematic of the Terahertz-Time Domain Spectroscopy (THz-TDS) system.

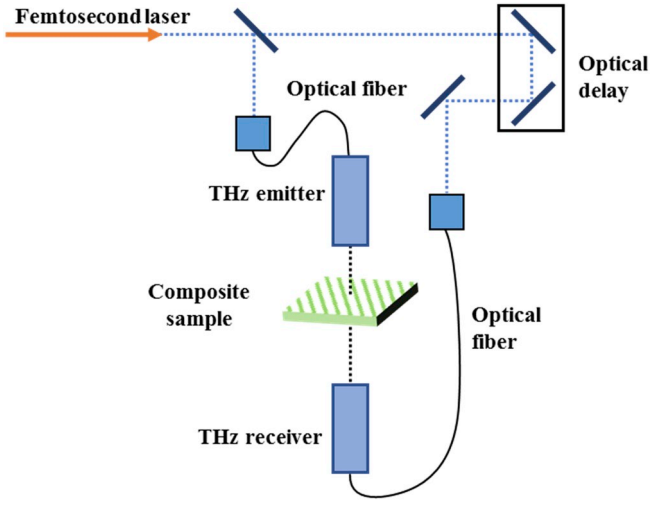

Fig. 3. Diagram of transmission mode with 0° incidence angle of THz-TDS system.

can be extracted using the electric field data ($E(\omega)$) measured by the sample and the reference as a ratio:

$$\frac{E_{sample}}{E_{ref}} = A\, e^{-i\phi(\omega)} \tag{2}$$

The complex relative refractive index ($\underline{n}$) is usually expressed as

Table 1
Material information of E-glass/epoxy pre-impregnated material (UGN160B).

Properties	Value
Ply thickness (mm)	0.136
Resin content (%)	33
Fiber Areal Wt. (g/m^3)	160
Density of E-glass fiber (kg/m^3)	2.54×10^3
Density of epoxy resin	1.2×10^3

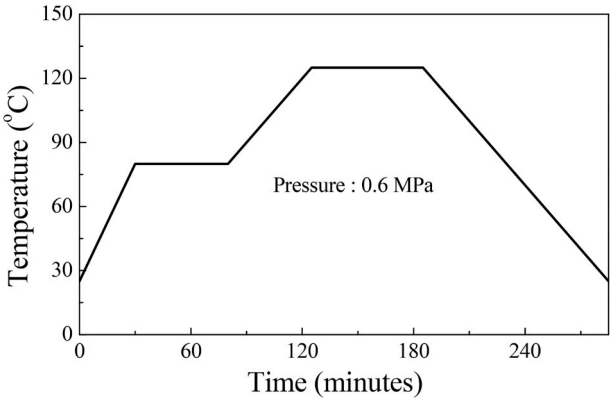

Fig. 4. Curing cycle of the GFRP specimen production for a vacuum bagging.

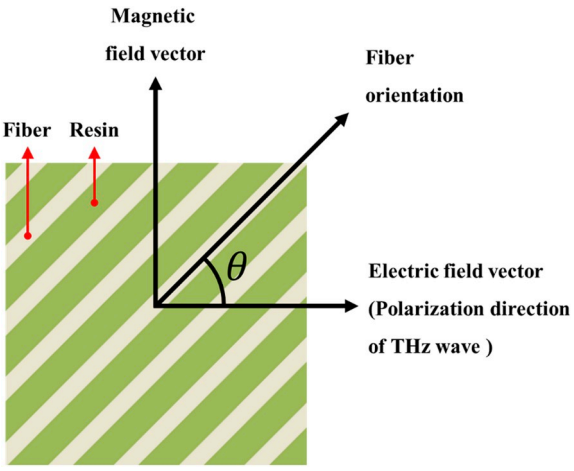

Fig. 5. The schematic diagram of the polarization direction of THz wave and fiber direction of the GFRP composite for measurement.

$$\underline{n}(\omega) = \frac{C}{\omega d}\phi + 1 \tag{3}$$

The under-bar notation denotes complex quantities. C is the velocity of THz wave, and d is the composites thickness. The complex relative refractive index ($\underline{n}$) and complex relative permittivity ($\underline{\varepsilon}_r$) have the following relationship [46]:

$$\underline{\varepsilon}_r = [\underline{n}(\omega)]^2 \tag{4}$$

Since the GFRP composites are dielectric material with low-dissipation properties, this relation is valid. The complex relative permittivity is a complex number composed of a real part, $\varepsilon_r^{'}$ (dielectric constant), and an imaginary part, $\varepsilon_r^{''}$ (imaginary permittivity).

$$\underline{\varepsilon}_r = \varepsilon_r^{'} - i\varepsilon_r^{''} = \varepsilon_r^{'}(1 - i\tan\delta) \tag{5}$$

The dielectric constant is related to the energy storage in dielectric materials, and the imaginary permittivity is related to the energy dissipation. The tan δ, the ratio of the imaginary permittivity to dielectric constant, is the dielectric loss tangent, which represents the energy loss [47].

3.2. Estimating the dielectric constant of unidirectional GFRP composite

Due to low dissipation properties, the dielectric constants of the GFRP composite could be analyzed to investigate the relation between the polarized direction of THz radiation and fiber direction. Depending on the polarized direction of the THz radiation, the dielectric constant of unidirectional GFRP composite varies. Based on this fact, a two-dimensional matrix can demonstrate the dielectric constants of unidirectional GFRP composite, as follows [48]:

$$[\varepsilon'_{ij}] = \begin{bmatrix} \varepsilon'_{11} & 0 \\ 0 & \varepsilon'_{22} \end{bmatrix} \tag{6}$$

where ε'_{11} and ε'_{22} denote the dielectric constants measured when the polarization angle of THz radiation is parallel to the fiber orientation ($\theta = 0°$) of GFRP composite and perpendicular to the fiber orientation ($\theta = 90°$), respectively. Since the electric field of the THz wave is polarized in single direction, the interaction between ε'_{11} and ε'_{22} could not be considered, so that the values of ε'_{12} and ε'_{21} are zero.

To estimate dielectric behavior with respect to the polarization angle (θ) of THz radiation to the fiber direction of composite, a transformation matrix that was bound with a direction cosine matrix for the second-order tensor was suggested, as follows:

$$[\varepsilon'_{ij}]^{\theta} = \begin{bmatrix} \cos\theta & \sin\theta \\ -\sin\theta & \cos\theta \end{bmatrix} \begin{bmatrix} \varepsilon'_{11} & 0 \\ 0 & \varepsilon'_{22} \end{bmatrix} \begin{bmatrix} \cos\theta & -\sin\theta \\ \sin\theta & \cos\theta \end{bmatrix} \tag{7}$$

where $[\varepsilon'_{ij}]^{\theta}$ is the dielectric constants of the laminated composites when the polarization angle of the THz radiation to the fiber direction of the composite is θ. For low-loss unidirectional polymeric composites, the dielectric constant for polarization angle (θ) can be estimated by substituting the values of ε'_{11} and ε'_{22} into Eq. (7).

3.3. Estimating the dielectric constants of a laminated composite with an arbitrary stacking sequence

To estimate the dielectric constants of composite based on its composition, a laminating rule derived from an AC circuit model composited of parallel capacitances and resistances was used and is expressed as follows [49]:

$$\varepsilon_{eq}^{'} = \frac{1}{d}\sum_{i=1}^{n} t_i \varepsilon_i^{'} \tag{8}$$

where ε'_{eq} and ε'_i are the dielectric constants of the entire composites and the i-th layer, respectively, and d and t_i are the thickness of the entire composite and the i-th layer, respectively. In AC circuit model, the dielectric constant of the individual GFRP composites layer was modeled as parallel to each other. Therefore, if the composition of stacking angle is same, total dielectric constant of the GFRP composite laminates would not change according to the stacking sequence of the individual layers.

Since the dielectric constants for the arbitrary stacking angle of each layer could be obtained by calculation of Eq. (7), the dielectric constants (ε'_{eq}) of GFRP composites in which n piles were stacked at arbitrary angle could be predicted for arbitrary polarization angle (θ) of the THz radiation to fiber direction by simply using Eq. (8).

4. Results and discussion

To verify the theories described at previous section, the time-domain data of the unidirectional GFRP composite specimen was measured, while the polarization angle (θ) of the THz radiation to the fiber direction of the composite was changed from 0° to 90° in 10° increments, as shown in Fig. 5. The time-domain data measured at the polarization angle $\theta = 0°$ and 90° to the fiber direction is shown in Fig. 6. The black line indicated the THz signal measured without composites sample. The

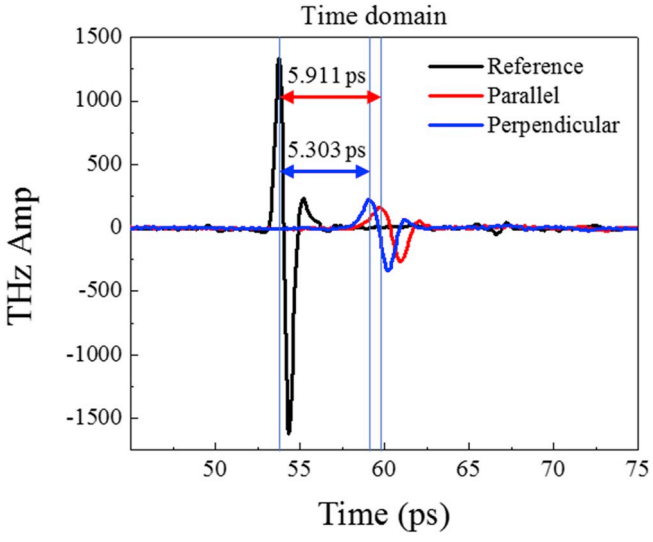

Fig. 6. The THz wave waveform in time-domain in case that the polarization angle of the THz radiation is parallel to fiber direction and perpendicular.

red and blue line indicated the THz signals transmitting the composite sample at the polarization angle θ = 0° (parallel) and 90° (perpendicular), respectively. The time-of-flight measured at the polarization angle θ = 0° and 90° is 5.911 ps and 5.303 ps, respectively. It was found that the value of time-of-flight measured at the polarization angle θ = 0° (parallel) was longer than that of the polarization angle θ = 90° (perpendicular). The difference of time-of-flight between parallel and perpendicular might be induced by the change of refractive index according to polarization angle of the THz radiation.

Frequency-domain data were obtained in the 0.2–0.8 THz range by the FFT of the measured time-domain data using Eq. (1). The magnitude (A) and phase (ϕ) of the THz wave transmitting the unidirectional GFRP composite at the polarization angle $\theta = 0^\circ$ were obtained using Eq. (2), and are shown in Fig. 7.

Then, the dielectric constants ($\varepsilon_r^{'}$), imaginary permittivity ($\varepsilon_r^{''}$) and loss tangent (tan δ) were calculated in the 0.2–0.8 THz frequency range by substituting the calculated magnitude and phase into Eqs. (3) and (4), respectively. The values of the dielectric constants, imaginary permittivity and the loss tangent at polarization angle $\theta = 0^\circ$ are shown in Fig. 8. It was found that the imaginary part of the complex permittivity and the loss tangent increased as the frequency increased, which means that the THz wave dissipated more at higher frequencies.

The calculation results of the complex permittivity and the loss tangent with respect to the polarization angle (θ) of the THz radiation to the fiber direction at 0.305 THz are shown in Table 2 and plotted in Fig. 9. It was found that the dielectric constants ($\varepsilon_r^{'}$) of the unidirectional GFRP composite decreased from 4.60536 to 4.01562, as the polarization angle of the THz radiation to the fiber direction increased. From 0° to 40°, the imaginary permittivity ($\varepsilon_r^{''}$) increased from 0.326804 to 0.400212, and then decreased again to 0.268635 until the polarization angle (θ) = 90°. Similarly, the loss tangents increased from 0.0709616 to 0.0919104 until $\theta = 40^\circ$, then decreased to 0.0668975 at $\theta = 90^\circ$. This means that the THz wave dissipated more as the polarization angle of the THz radiation to the fiber direction increased.

To investigate in detail the variation of dielectric constant with respect to the polarization angle (θ), the dielectric constant of unidirectional GFRP composite was expressed as the relationship between the refractive index (n) and the extinction coefficient (κ) of the complex relative refractive index, as shown below [46]:

$$\varepsilon_r^{'} = n^2 - \kappa^2 \tag{9}$$

where n and κ are the real and imaginary part of the complex relative refractive index, respectively. As listed in Table 3, the refractive index (n) and extinction coefficient (κ) of unidirectional GFRP composite were measured as 2.147 and 0.0761, respectively, when the polarization angle (θ) of the THz radiation was 0° at 0.305 THz. Also, the refractive index and extinction coefficient at the polarization angle $\theta = 90^\circ$ at 0.305 THz were 2.005 and 0.0670, respectively. The ratio of the refractive index and extinction coefficient is 28.2 and 29.9 respectively. Since the refractive index (n) of GFRP composite was about 30 times greater than its extinction coefficient (κ), the change of the dielectric constant was dominantly influenced by the change of the refractive index.

Our previous research [50] confirmed that the refractive index of glass fiber composites was larger when the fiber direction and polarization vector were parallel to each other, rather than perpendicular. From this fact, it could be concluded that the values of the dielectric constant were influenced by the polarization angle (θ) of the THz radiation to the fiber direction. Also, the fact that the time-of-flight in time-domain data is different between the polarization angle (θ) = 0° and 90° was confirmed to be induced by difference of the refractive index depending on the polarization angle. Furthermore, the dielectric constants of the GFRP composites were found to decrease as the polarization angle (θ) of the THz radiation to the fiber direction wave increased (Fig. 9 (a)).

To estimate the dielectric constants of the unidirectional GFRP composite for an arbitrary polarization angle (θ) of the THz radiation, the transformation equation was introduced, which was expressed in Eq. (7). By substituting the measured dielectric constants given in Table 2 ($\varepsilon_{11}^{'} = 4.60536$ and $\varepsilon_{22}^{'} = 4.01562$) into Eq. (7), the dielectric constants for the polarization angle (θ) of the THz radiation were calculated from 0° to 90°. The calculation results of dielectric constants were compared with measurement results, as shown in Fig. 9 (a) and Table 4. It was confirmed that the dielectric constants calculated by the transformation matrix were in good agreement with the measured ones.

From the comparison, it was found that the transformation equation could predict the dielectric constants of the unidirectional GFRP composites at an arbitrary polarization angle of the THz radiation to the fiber direction of the composites with maximum errors of about 1%. This indicates that the dielectric constants of the unidirectional GFRP composites at an arbitrary polarization angle of the THz radiation could be predicted by transforming $\varepsilon_{11}^{'}$ and $\varepsilon_{22}^{'}$.

To verify the rule for estimating the dielectric constant of the GFRP composite laminates with an arbitrary stacking sequence, the GFRP composite laminates specimen were prepared with $[\pm 30^\circ]_{3s}$, $[+45^\circ/0^\circ/-45^\circ]_{2s}$, and $[+60^\circ/0^\circ/-60^\circ]_{2s}$ stacking sequences. Then, those dielectric constants in the 0.2–0.8 THz frequency range were measured, while the polarization angle of the THz radiation to the global laminate coordinate was changed from 0° to 90° in 10° increments.

By substituting the dielectric constants ($\varepsilon_{11}^{'}$ and $\varepsilon_{22}^{'}$) of the unidirectional GFRP composite into Eq. (7), the dielectric constants of unidirectional GFRP were calculated with respect to the polarization angle (θ) of the THz radiation from 0° to 90° in the 0.2–0.8 THz frequency range. To calculate the dielectric constants (ε'_{eq}) for the $[\pm 30^\circ]_{3s}$,

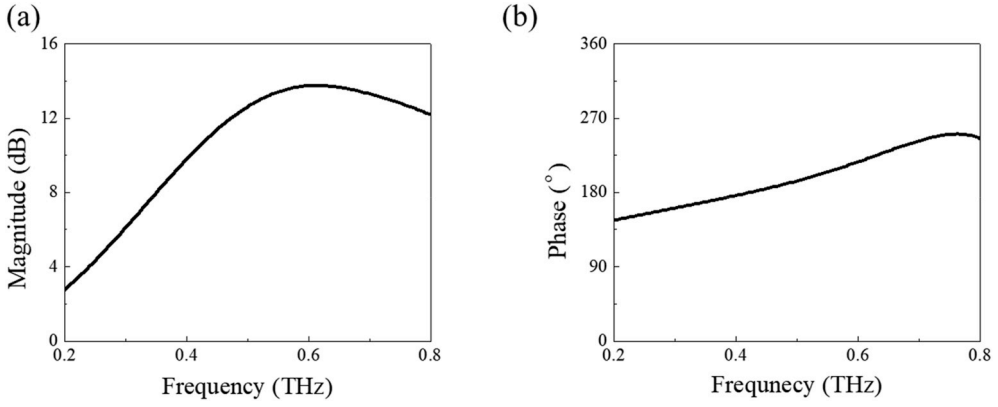

Fig. 7. (a)Magnitude and (b)phase of THz wave through the unidirectional GFRP composite specimen in frequency range of 0.2–0.8 THz when the polarization angle (θ) is 0°.

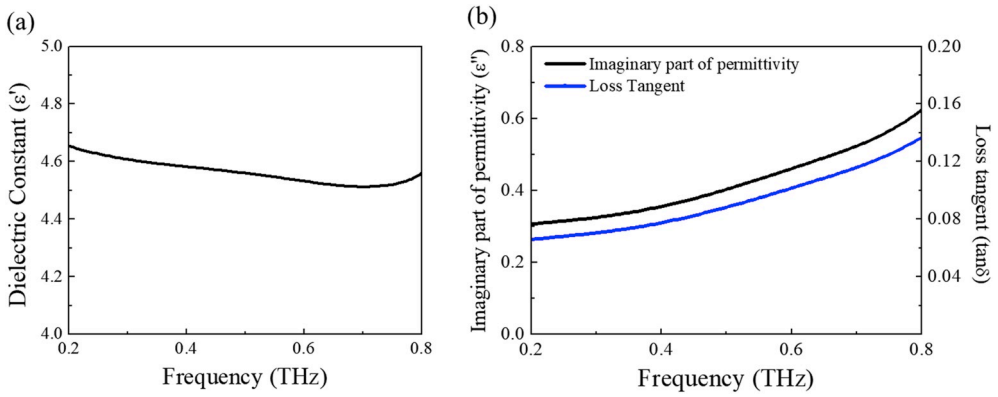

Fig. 8. The measurement results of (a) Dielectric constant and (b) imaginary permittivity, and loss tangent of the unidirectional GFRP composite in frequency range of 0.2–0.8 THz when the polarization angle (θ) is 0°.

Table 2
The measurement results of the complex permittivity of the unidirectional GFRP composite at 0.305 THz, while polarization angle of the THz radiation to fiber direction of composite was changed with the increment of 10° from 0° to 90°.

Angle (°)	Dielectric Constant (ε')	Imaginary permittivity (ε'')	Loss tangent (tanδ)
0	4.60536	0.326804	0.0709616
10	4.58025	0.343114	0.0749116
20	4.53979	0.370537	0.0816199
30	4.46075	0.398476	0.0893294
40	4.35437	0.400212	0.0919104
50	4.25519	0.372155	0.0874591
60	4.15956	0.331970	0.0798089
70	4.08342	0.300139	0.0735019
80	4.03390	0.275887	0.0683921
90	4.01562	0.268635	0.0668975

$[+45°/0°/-45°]_{2s}$, and $[+60°/0°/-60°]_{2s}$ stacking sequences, the dielectric constants calculated with respect to the polarization angle (θ) of the THz radiation above were substituted into Eq. (8) as the dielectric constant of each layer (ε'_i).

Fig. 10 compares the results of the calculated and the measured data for the dielectric constants of the $[\pm30°]_{3s}$, $[+45°/0°/-45°]_{2s}$, and $[+60°/0°/-60°]_{2s}$ stacking sequences in the 0.2–0.8 THz range frequency, when the polarization angle (θ) of the THz radiation to the laminates coordinates of composites was 0°. It was observed that the calculated results were in good agreement with the measured results through the entire 0.2–0.8 THz range. The experimental results and the estimated results were slightly different. This might be due to the scattering effect of the THz radiation in the interface between layers.

Table 5 and Fig. 11 show the dielectric constants of four different GFRP composite specimens (unidirectional laminate, $[\pm30°]_{3s}$, $[+45°/0°/-45°]_{2s}$, and $[+60°/0°/-60°]_{2s}$ stacking sequences) with respect to the polarization angle (θ) of the THz radiation, when the frequency was 0.305 THz. As listed in Table 5, the measured dielectric constants of the angle ply laminates of the $[\pm30°]_{3s}$, $[+45°/0°/-45°]_{2s}$, and $[+60°/0°/-60°]_{2s}$ stacking sequences were in the ranges of 4.15810–4.44682, 4.21036–4.40674, and 4.30353–4.31466, respectively. As shown in Fig. 11, the dielectric constants of the $[\pm30°]_{3s}$ and $[+45°/0°/-45°]_{2s}$ stacking sequence composites continuously decreased as the polarization angle (θ) of the THz radiation increased from 0° to 90°, similar to the tendency of the unidirectional GFRP composites.

It is noteworthy that in the case of the $[+60°/0°/-60°]_{2s}$ stacking

Table 3
The calculation result of refractive index, extinction coefficient and the ratio the extinction coefficient to refractive index in cases that in case that the polarization angle of the THz radiation is parallel to fiber direction and perpendicular at 0.305 THz.

The polarization angle of the THz radiation to the fiber direction (θ)	Refractive index (n)	Extinction coefficient (κ)	Ratio (n/κ)
Parallel ($\theta = 0°$)	2.147	0.0761	28.2
Perpendicular ($\theta = 90°$)	2.005	0.0670	29.9

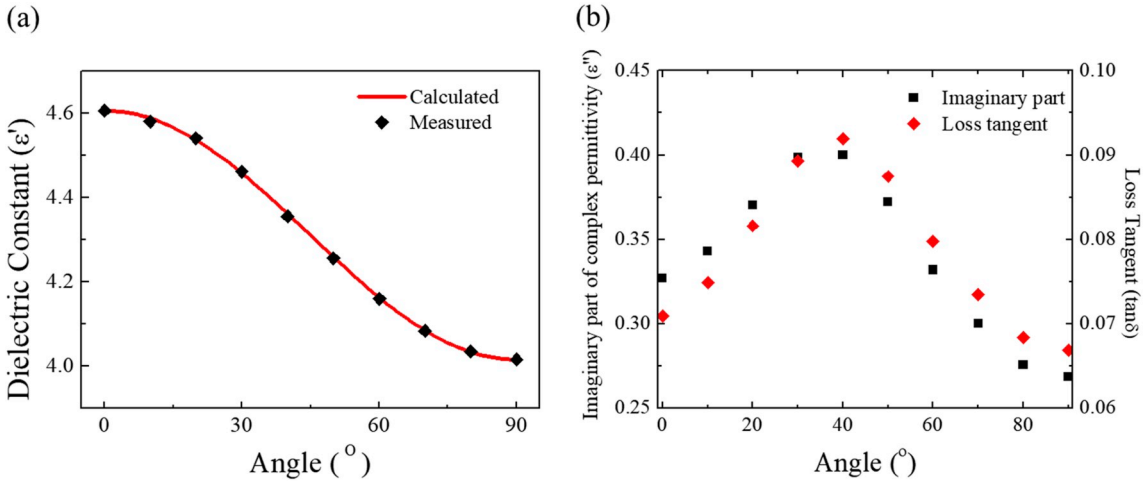

Fig. 9. (a) The measurement and calculation results of the dielectric constant and (b) the measurement results of imaginary permittivity, and loss tangent of the unidirectional GFRP composite with respect to polarization angle (θ) at 0.305 THz frequency.

Table 4
The comparison measured dielectric constant with calculated one of the unidirectional GFRP composite with the increment of 10° from 0° to 90° at 0.305 THz.

Angle(°)	Dielectric Constant (ε')	
	Measured	Calculated
0	4.60536	4.60476
10	4.58025	4.58696
20	4.53979	4.53570
30	4.46075	4.45716
40	4.35437	4.36081
50	4.25519	4.25828
60	4.15956	4.16194
70	4.08342	4.08340
80	4.03390	4.03214
90	4.01562	4.01433

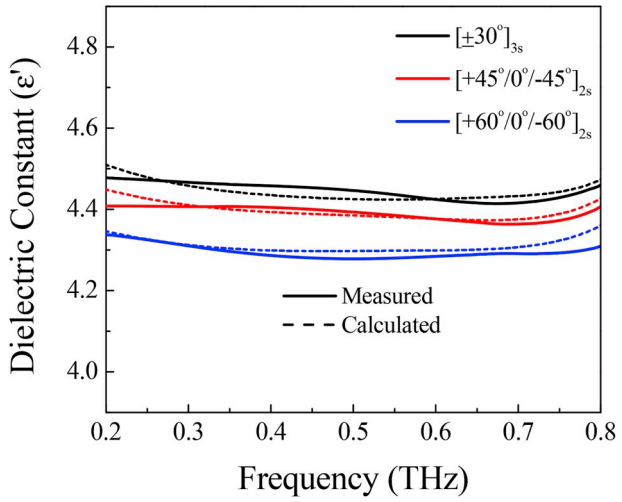

Fig. 10. The comparison of the measurement and calculation results for dielectric constants of the angle ply laminate of $[\pm30°]_{3s}$, $[+45°/0°/-45°]_{2s}$, and $[+60°/0°/-60°]_{2s}$ stacking sequence in the frequency range of 0.2–0.8 THz.

sequence, which is a quasi-isotropic laminate, the dielectric constants were constant, regardless of the polarization angle of the THz radiation to the fiber direction of the composite, similar to its quasi-isotropic mechanical behavior. From the comparison results, it can be concluded that the dielectric constants of the GFRP composite laminates with an arbitrary laminating sequence could be predicted with a maximum error of about 0.25% using the THz-TDS system. This method can be widely used to inspect the fiber direction after composite manufacturing process and to improve its service life and maintenance.

5. Conclusion

The dielectric constants of GFRP composite laminates with various stacking sequences were measured by a THz-TDS system by changing the polarization direction of the THz radiation to the fiber direction of the composite from 0° to 90° in 10° increments. The interaction between the polarization angle of the THz radiation and the fiber direction was experimentally and analytically obtained. The dielectric constants of the unidirectional GFRP composites were calculated with respect to the polarization angle (θ) of the THz radiation using the transformation equation that could predict the dielectric constants with a maximum error of 1.0%. Additionally, the rule for predicting dielectric constants of arbitrarily laminated composites was verified with the data measured in the $[\pm30°]_{3s}$, $[+45°/0°/-45°]_{2s}$, and $[+60°/0°/-60°]_{2s}$ stacking sequences, and the dielectric constants could be predicted with a maximum error of 0.25%. The investigation indicated that the fiber-direction distortion could be detected in the composite manufacturing process and during maintenance.

Declarations of interest

None.

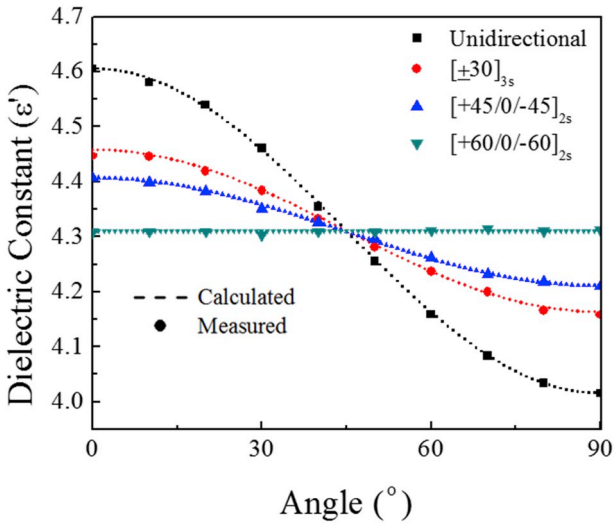

Fig. 11. Comparison of measurement and calculation results for the dielectric constants of four different composite specimens at 0.305 THz while polarization angle of the THz radiation to fiber direction of composite was changed from 0° to 90°.

Table 5
The comparison measured dielectric constants with calculated ones of $[\pm30°]_{3s}$, $[+45°/0°/-45°]_{2s}$, and $[+60°/0°/-60°]_{3s}$ stacking sequence GFRP composites with the increment of 10° from 0° to 90°

Angle(°)	Dielectric Constant (ε')					
	$[\pm30°]_{3s}$		$[+45°/0°/-45°]_{2s}$		$[+60°/0°/-60°]_{2s}$	
	Measured	Calculated	Measured	Calculated	Measured	Calculated
0	4.44682	4.45793	4.40674	4.40739	4.30918	4.31049
10	4.44563	4.44904	4.39930	4.40149	4.30994	4.31049
20	4.41944	4.42343	4.38235	4.38448	4.30959	4.31049
30	4.38425	4.38421	4.35120	4.35842	4.30353	4.31049
40	4.33274	4.33609	4.32576	4.32646	4.30944	4.31049
50	4.28124	4.28489	4.29611	4.29244	4.30834	4.31049
60	4.23687	4.23677	4.26216	4.26048	4.31162	4.31049
70	4.19905	4.19755	4.23257	4.23442	4.31466	4.31049
80	4.16609	4.17195	4.21841	4.21741	4.31035	4.31049
90	4.15810	4.16305	4.21036	4.21151	4.31224	4.31049

Acknowledgments

This research was supported by a National Research Foundation of Korea grant funded by the Korean Government (MEST) (2012R1A6A1029029, 2013M2A2A9043280, and 2018R1D1A1A09083236).

References

[1] Al-saadi AU, Aravinthan T, Lokuge W. Structural applications of fibre reinforced polymer (FRP) composite tubes: a review of columns members. Compos Struct 2018;204:513–24.
[2] Hussain A, Calabria-Holley J, Lawrence M, Ansell MP, Jiang Y, Schorr D, et al. Development of novel building composites based on hemp and multi-functional silica matrix. Composites Part B 2019;156:266–73.
[3] Zhu D, Shi H, Fang H, Liu W, Qi Y, Bai Y. Fiber reinforced composites sandwich panels with web reinforced wood core for building floor applications. Composites Part B 2018;150:196–211.
[4] Dong H, Li Z, Wang J, Karihaloo B. A new fatigue failure theory for multidirectional fiber-reinforced composite laminates with arbitrary stacking sequence. Int J Fatigue 2016;87:294–300.
[5] Manimaran P, Senthamaraikannan P, Sanjay M, Marichelvam M, Jawaid M. Study on characterization of Furcraea foetida new natural fiber as composite reinforcement for lightweight applications. Carbohydr Polym 2018;181:650–8.
[6] Mortazavian S, Fatemi A. Effects of fiber orientation and anisotropy on tensile strength and elastic modulus of short fiber reinforced polymer composites. Composites Part B 2015;72:116–29.
[7] Ning F, Cong W, Qiu J, Wei J, Wang S. Additive manufacturing of carbon fiber reinforced thermoplastic composites using fused deposition modeling. Composites Part B 2015;80:369–78.
[8] Portella EH, Romanzini D, Angrizani CC, Amico SC, Zattera AJ. Influence of stacking sequence on the mechanical and dynamic mechanical properties of cotton/glass fiber reinforced polyester composites. Mater Res 2016;19(3):542–7.
[9] Shirvanimoghaddam K, Hamim SU, Akbari MK, Fakhrhoseini SM, Khayyam H, Pakseresht AH, et al. Carbon fiber reinforced metal matrix composites: fabrication processes and properties. Composites Part A 2017;92:70–96.
[10] Yuchang Q, Jie W, Hongyu W, Fa L, Wancheng Z. Graphene nanosheets/E-glass/epoxy composites with enhanced mechanical and electromagnetic performance. RSC Adv 2016;6(84):80424–30.
[11] Kim D-H, Kim H-G, Kim H-S. Design optimization and manufacture of hybrid glass/carbon fiber reinforced composite bumper beam for automobile vehicle. Compos Struct 2015;131:742–52.
[12] Kim D-H, Jung K-H, Kim D-J, Park S-H, Kim D-H, Lim J, et al. Improving pedestrian safety via the optimization of composite hood structures for automobiles based on the equivalent static load method. Compos Struct 2017;176:780–9.
[13] Shokrieh MM, Rezaei D. Analysis and optimization of a composite leaf spring. Compos Struct 2003;60(3):317–25.
[14] Keller A, Dransfeld C, Masania K. Flow and heat transfer during compression resin transfer moulding of highly reactive epoxies. Composites Part B 2018;153:167–75.
[15] Kim J-H, Kwon D-J, Shin P-S, Beak Y-M, Park H-S, DeVries KL, et al. Interfacial properties and permeability of three patterned glass fiber/epoxy composites by VARTM. Composites Part B 2018;148:61–7.
[16] Allen YY, Huang C, Klocke F, Brecher C, Pongs G, Winterschladen M, et al. Development of a compression molding process for three-dimensional tailored free-form glass optics. Appl Opt 2006;45(25):6511–8.
[17] Kim D-J, Yu M-H, Lim J, Nam B, Kim H-S. Prediction of the mechanical behavior of fiber-reinforced composite structure considering its shear angle distribution generated during thermo-compression molding process. Compos Struct 2019;220:441–50.
[18] Kang H, Shan Z, Zang Y, Liu F. Effect of yarn distortion on the mechanical properties of fiber-bar composites reinforced by three-dimensional weaving. Appl Compos Mater 2016;23(2):119–38.
[19] Ganapathi A, Joshi SC, Chen Z. Flow-compacted deformations coupled with thermo-chemically induced distortions in manufacturing of thick unidirectional carbon fiber reinforced plastics composites. J Compos Mater 2016;50(24):3325–43.
[20] Gholizadeh S. A review of non-destructive testing methods of composite materials. Procedia Struct Integr 2016;1:50–7.
[21] Sutthaweekul R, Tian GY, Wang Z, Ciampa F. Microwave open-ended waveguide for detection and characterisation of FBHs in coated GFRP pipes. Compos Struct 2019:111080.
[22] Segers J, Hedayatrasa S, Verboven E, Poelman G, Van Paepegem W, Kersemans M. In-plane local defect resonances for efficient vibrothermography of impacted carbon fiber reinforced plastics. NDT Int 2019;102:218–25.
[23] Nelson L, Smith R. Fibre direction and stacking sequence measurement in carbon fibre composites using Radon transforms of ultrasonic data. Composites Part A 2019;118:1–8.
[24] Fernandes H, Zhang H, Ibarra-Castanedo C, Maldague X. Fiber orientation assessment on randomly-oriented strand composites by means of infrared thermography. Compos Sci Technol 2015;121:25–33.
[25] Chu Z, Cheng H, Zhou Y, Wang Q, Wang J. Anisotropic microwave absorbing properties of oriented SiC short fiber sheets. Mater Des 2010;31(6):3140–5.
[26] Naito K, Kagawa Y, Kurihara K. Dielectric properties and noncontact damage detection of plain-woven fabric glass fiber reinforced epoxy matrix composites using millimeter wavelength microwave. Compos Struct 2012;94(2):695–701.
[27] Seo D-W, Kim H-J, Bae K-U, Myung N-H. The effect of fiber orientation distribution on the effective permittivity of fiber composite materials. J. Electromagn. Waves Appl. 2010;24(17–18):2419–30.
[28] Krause M, Hausherr J-M, Burgeth B, Herrmann C, Krenkel W. Determination of the fibre orientation in composites using the structure tensor and local X-ray transform. J Mater Sci 2010;45(4):888–96.
[29] Thi TBN, Morioka M, Yokoyama A, Hamanaka S, Yamashita K, Nonomura C. Measurement of fiber orientation distribution in injection-molded short-glass-fiber composites using X-ray computed tomography. J Mater Process Technol 2015;219:1–9.
[30] Urabe K, Yomoda S. A nondestructive testing method of fiber orientation by microwave. Adv Compos Mater 1991;1(3):193–208.
[31] Buccheri F, Zhang X-C. Terahertz emission from laser-induced microplasma in ambient air. Optica 2015;2(4):366–9.
[32] Rahani EK, Kundu T, Wu Z, Xin H. Mechanical damage detection in polymer tiles by THz radiation. IEEE Sens J 2011;11(8):1720–5.
[33] Dong J, Kim B, Locquet A, McKeon P, Declercq N, Citrin D. Nondestructive evaluation of forced delamination in glass fiber-reinforced composites by terahertz and ultrasonic waves. Composites Part B 2015;79:667–75.
[34] Palka N, Panowicz R, Chalimoniuk M, Beigang R. Non-destructive evaluation of puncture region in polyethylene composite by terahertz and X-ray radiation. Composites Part B 2016;92:315–25.
[35] Dandolo CLK, Lopez M, Fukunaga K, Ueno Y, Pillay R, Giovannacci D, et al. Toward a multimodal fusion of layered cultural object images: complementarity of optical coherence tomography and terahertz time-domain imaging in the heritage field. Appl Opt 2019;58(5):1281–90.
[36] Dong J, Pomarède P, Chehami L, Locquet A, Meraghni F, Declercq NF, et al. Visualization of subsurface damage in woven carbon fiber-reinforced composites using polarization-sensitive terahertz imaging. NDT Int 2018;99:72–9.
[37] Cheon H, Yang H-J, Lee S-H, Kim YA, Son J-H. Terahertz molecular resonance of cancer DNA. Sci Rep 2016;6:37103.
[38] Knipper R, Brahm A, Heinz E, May T, Notni G, Meyer H-G, et al. THz absorption in fabric and its impact on body scanning for security application. IEEE Trans Terahertz Sci Technol 2015;5(6):999–1004.
[39] Dong J, Locquet A, Declercq NF, Citrin D. Polarization-resolved terahertz imaging of intra-and inter-laminar damages in hybrid fiber-reinforced composite laminate subject to low-velocity impact. Composites Part B 2016;92:167–74.
[40] Shin HJ, Choi S-W, Ok G. Qualitative identification of food materials by complex refractive index mapping in the terahertz range. Food Chem 2018;245:282–8.
[41] Park D-W, Oh G-H, Kim D-J, Kim H-S. In-situ thickness measurement of epoxy molding compound in semiconductor package products using a terahertz-time of flight system. NDT Int 2019;105:11–8.
[42] Zolliker P, Rüggeberg M, Valzania L, Hack E. Extracting wood properties from structured THz spectra: birefringence and water content. IEEE Trans Terahertz Sci Technol 2017;7(6):722–31.
[43] Jördens C, Wietzke S, Scheller M, Koch M. Investigation of the water absorption in polyamide and wood plastic composite by terahertz time-domain spectroscopy. Polym Test 2010;29(2):209–15.
[44] Scalettar B, Swedlow J, Sedat J, Agard D. Dispersion, aberration and deconvolution in multi-wavelength fluorescence images. J Microsc 1996;182(1):50–60.
[45] Brucherseifer M, Nagel M, Haring Bolivar P, Kurz H, Bosserhoff A, Büttner R. Label-free probing of the binding state of DNA by time-domain terahertz sensing. Appl Phys Lett 2000;77(24):4049–51.
[46] Afsar MN, Chi H. Millimeter wave complex refractive index, complex dielectric permittivity and loss tangent of extra high purity and compensated silicon. Int J Infrared Millim Waves 1994;15(7):1181–8.
[47] Teo M, Kong L, Li Z, Lin G, Gan Y. Development of magneto-dielectric materials based on Li-ferrite ceramics: II. DC resistivity and complex relative permittivity. J Alloy Comp 2008;459(1–2):567–75.
[48] Seo IS, Chin WS. Characterization of electromagnetic properties of polymeric composite materials with free space method. Compos Struct 2004;66(1–4):533–42.
[49] Chin WS. Laminating rule for predicting the dielectric properties of E-glass/epoxy laminate composite. Compos Struct 2007;77(3):373–82.
[50] Oh G-H, Jeong J-H, Park S-H, Kim H-S. Terahertz time-domain spectroscopy of weld line defects formed during an injection moulding process. Compos Sci Technol 2018;157:67–77.